Trends in
Plant Biology

Trends in Plant Biology, 2025, 2:1–14

RESEARCH ARTICLE OPEN ACCESS

CCS52A1/2 orchestrate hypocotyl endoreplication and elongation via PKN1/PKN2 pathways in *Arabidopsis thaliana*

Lei Li[1,2*] | Tangnur Kaderbek[3]

[1]Department of Plant Biotechnology and Bioinformatics, Ghent University, 9052 Ghent, Belgium | [2]Key Laboratory of Plant Development and Environmental Adaptation Biology, Ministry of Education, School of Life Sciences, Shandong University, Qingdao, Shandong 266237, China | [3]Frontiers Science Center for Molecular Design Breeding (MOE), State Key Laboratory of Maize Bio-breeding, National Maize Improvement Center, Department of Plant Genetics and Breeding, China Agricultural University, Beijing, China

*Correspondence: lilei415@sdu.edu.cn (LL)

Received 10 November 2024 | **Revised** 26 January 2025 | **Accepted** 11 February 2025 | **Published online** 21 February 2025

ABSTRACT

Etiolated hypocotyls undergo rapid elongation compared with light-grown seedlings, a process associated with a developmental transition from mitotic cell division to endoreplication, resulting in increased cellular ploidy. *CELL CYCLE SWITCH 52A2* (*CCS52A2*) is a key regulator of endoreplication in *Arabidopsis thaliana*, functioning through activation of the anaphase-promoting complex/cyclosome (APC/C) to mediate cyclin degradation. In this study, we demonstrate that loss-of-function mutations in *CCS52A2* significantly reduce hypocotyl elongation, particularly under dark-grown (etiolated) conditions. Notably, this phenotype is partially rescued in a *ccs52a2 pkn1* double mutant, indicating that *CCS52A2* promotes etiolated hypocotyl elongation at least in part through the PKN1 signaling pathway. Furthermore, our findings suggest that endoreplication influences cell wall composition and its downstream modifications, providing new insight into the link between ploidy level and cell wall dynamics during skotomorphogenic growth.

Keywords: *CELL CYCLE SWITCH 52A2 (CCS52A2)* | Cell expansion | Cell wall | Hypocotyl elongation | Lignin biosynthesis

1 | INTRODUCTION

The hypocotyl serves as an embryonic stem organ that promotes plant growth by linking the cotyledons to the underground root system [1]. During the post-germination stage, the hypocotyl rapidly elongates to penetrate the soil and capture the light signal, accompanied by a significant increase in cell size in the hypocotyl epidermal cells, especially under dark-grown conditions. In addition, the cell ploidy level of etiolated hypocotyl cells is higher than that of light-grown seedlings, a process named endoreplication [2,3]. Morphological studies have shown that during post-germination growth, the elongation speed of hypocotyl epidermal cells, grown under light, increases first in the bottom part and then in the top part of the hypocotyl [4]. In addition, under dark-grown conditions, the epidermal cells of the bottom part of the hypocotyl elongate more rapidly, at an early stage, and later the epidermal cells of the middle part of the hypocotyl exhibit the highest elongation speed [5]. Multiple hormones are known to participate in *Arabidopsis* hypocotyl development [1,6]. For example, gibberellic acid (GA) has been identified to promote hypocotyl cell elongation via weakening of the cell wall [7,8]. Auxin has been found to play a positive role in cell expansion by activating cell wall acidification, thus loosening the cell wall and decreasing its thickness in the hypocotyl [9]. A recent study has revealed that auxin plays a dual role in regulating the development of etiolated hypocotyls in *Arabidopsis*. The study found that high levels of auxin initially suppress hypocotyl elongation immediately after germination. The asymmetrical distribution of internal auxin triggers the formation of the hypocotyl apical hook by activating the expression of *PP2*C.D1, a phosphatase that activates plasma membrane (PM) H^+-ATPases [10]. Later, the role of auxin in regulating hypocotyl elongation switches from negative to positive, coinciding with a decrease in internal auxin levels [11]. Furthermore, no endoreplication defect was detected in several auxin biosynthesis mutant hypocotyls [12], but the auxin polar transport mutant, *abcb19*, displays enhanced endoreplication in the hypocotyl [13]. These data indicate that the role of auxin in modulating the hypocotyl endocycle is complex.

The repression of *CDKs/Cyclin* complexes is a prerequisite for endoreplication. In *Arabidopsis*, *SIM/SMRs* and *CCS52A1/2* play positive roles in controlling endoreplication by inhibiting CDKs activity and activating the APC/C complex to degrade cyclins, respectively [14,15]. Genetic studies have shown that SIM controls endoreplication in *Arabidopsis* trichomes via repression CDK activity [16,17]. Its mutation generates multicellular trichomes with a lower ploidy level [14]. Similarly, mutation and overexpression of *SMR1* (LGO) repress and promote endocycle onset in leaf cells, respectively. Additionally, *SMR2*, a homolog of the SIM/SMRs family, has been observed to act as a positive factor in endoreplication onset [18]. *CCS52A1/2* have been identified as major factors in *Arabidopsis* endoreplication establishment [15,19,20].

Previously, *CYCA2;3* was identified as a downstream target of the $APC/C^{CCS52A1}$ complex, which controls the mitosis-endocycle transition [21]. In addition, our lab has identified two downstream targets of the $APC/C^{CCS52A2}$ complex through an EMS mutagenesis screen: *PKN1* (*AT2G43990*) and *PKN2* (*CYCA3;4*) [22,23]. After crossing with either *pkn1* or *pkn2* single mutants, a significant

recovery in the root growth defect of the *ccs52a2* mutant was observed [22,23]. ULTRAVIOLET-B-INSENSITIVE4 (UVI4) and DP-E2F-like 1 (DEL1) were identified as repressors of CCS52A1 and CCS52A2, respectively [24]. DEL1 acts as a negative regulator of endoreplication in *Arabidopsis* [25]. It has been identified as a positive and negative downstream target of E2Fb and E2Fc, respectively [26].

Cell wall activities during endoreplication represent a novel research focus [27], probably linked to cell morphological modifications, such as cell expansion. In addition, transcripts of cell wall biosynthesis and modification genes are enriched in the endoploidy cells [28–30]. ESKIMO1-5 (ESK1-5) encodes a major xylan acetyltransferase [31]. In the *esk1* mutant, xylan and mannan in vessels have low acetylation levels, resulting in dwarf growth due to collapsed vessels. However, this phenotype can be rescued by crossing with *kaktus* (*kak*) [32], which is an endoreplication repressor [33]. This provides evidence for a potential link between endoreplication and cell wall modifications. Moreover, endoreplication has been identified to be involved in the immunity process and accompanied by cell wall modifications, which were observed in the *smr1* and *sim smr1* mutants [34,35]. Furthermore, the composition of the cell wall in polyploid lines differs from that in diploid lines. *Arabidopsis* polyploid lines have higher contents of pectin and hemicellulose, and a lower contents of lignin and cellulose [36]. Additionally, the cell wall in polyploid etiolated hypocotyl cells is more relaxed than that in diploid lines [5]. In addition, CCS52A2 has a potential link with endoreplication and pectin methylesterification during the hypocotyl apical hook formation [37]. These results indicate that the DNA content has a potential link with cell wall activities. However, detailed molecular evidence describing the effect of endoreplication on cell wall activities remains elusive. Hypocotyl epidermal cells are commonly used as a research model to study the relationship between endoreplication and cell expansion. Post-germination growth mainly relies on endoreplication and is easily characterized. This allows investigation of the connection between endoreplication and cell growth in a well-controlled and easily accessible system [38].

To investigate the effect of endoreplication triggered by SIM/SMRs and CCS52A1/2 on the *Arabidopsis* hypocotyl, we analyzed the cell volume and ploidy level of light- and dark-grown hypocotyl epidermal cells through MorphoGraphX (MGX) and flow cytometry, respectively. We used MGX to analyze cell volume changes in hypocotyl epidermal and cortex cells between wild type (WT) and endocycle-related mutants, including *sim*, *smr1*, *smr2*, *sim sm1*, *sim smr1 smr2*, *ccs52a1*, *ccs52a2*, *sim ccs52a1*, and *smr1 ccs52a1*. Combined with flow cytometric results from WT and these mutant hypocotyls, we linked endoreplication with cell volume in the light- and dark-grown hypocotyls.

2 | RESULTS

2.1 | Expression pattern of *SIM/SMRs* and *CCS52A1/2* in the *Arabidopsis* hypocotyl

Previous research has mainly focused on the roles of *SIM/SMR1* and *CCS52A1/2* in controlling endocycle onset in the *Arabidopsis* root and leaf [15–17]. *SMR2* has also been found to play a role in regulating the balance between mitosis and endocycle in *Arabidopsis* leaves [18]. To investigate the effects of these genes on hypocotyl growth, we first examined the GUS activities of transcriptional reporter lines (*SIM*, *SMR1*, and *SMR2*) and translational reporter lines (*CCS52A1* and *CCS52A2*) in light-grown hypocotyls at different time points (0, 3, 5, and 7 days) (Figure 1). The 0-day time point represents the embryonic stage without seed coat. Promoter-GUS activity of *SIM* was patchy in the embryonic root and the bottom part of the hypocotyl at the 0-day time point. Then the *SIM-GUS* signal mainly accumulated in the vascular cells, and gradually disappeared from 3-day to 5-day time point, to come back at the 7-day time point in the vascular cells. We did not detect an *SMR1-GUS* signal in embryonic seedlings at the 0-day time point, but a signal appeared in the hypocotyl vascular cells, together with a patchy expression in the ground tissue and epidermal cells at the bottom part of the hypocotyl from the 3-day to 7-day time points. Interestingly, at the 3-day time point, the *SMR1-GUS* signal was strongest in the inner side of the bent region of the hypocotyl. *SMR2* was constitutively strong and presented in the hypocotyl from 0-day to 7-day time point, suggesting that SMR2 may play a crucial role in hypocotyl development. We could not detect a clear *CCS52A1* and *CCS52A2* signal during the hypocotyl development process from 0-day to 7-day time point (Figure 1).

Furthermore, to analyze how *SIM*, *SMR1*, *SMR2*, *CCS52A1*, and *CCS52A2* regulate hypocotyl growth, we measured the hypocotyl length of the corresponding mutants under light- and dark-grown conditions (Figure 2). The results showed that *sim*, *smr1*, and *smr2* knock-out lines displayed no significant change in the hypocotyl length under light- and dark-grown conditions, compared to WT. The hypocotyl length of the *sim smr1* double mutant was shorter than WT under light-grown conditions, while it was longer than WT under dark-grown conditions. However, the hypocotyl length defect was recovered in the *sim smr1 smr2* triple mutant, both under light- and dark-grown conditions. The *ccs52a1* and *ccs52a2* mutants both displayed hypocotyl elongation defects under light-grown conditions. The *ccs52a1* etiolated hypocotyl length was unchanged compared to WT, while a great reduction in hypocotyl length was observed in the etiolated *ccs52a2* hypocotyl. The hypocotyl length of *sim ccs52a1* and *smr1 ccs52a1* was decreased compared to WT under light-grown conditions. However, under dark-grown conditions, *sim ccs52a1* displayed no significant changes in hypocotyl length, whereas the hypocotyl length of *smr1 ccs52a1* was increased compared to WT (Figure 2). This indicates that the crosstalk between *SMR1* and *CCS52A1* might be influenced by the light signaling.

As hypocotyl length is the result of cell length and number, we checked the light-grown hypocotyl epidermal cell number among these mutants and WT at the 7-day time point. The quantification was done on the basis of scanning electron microscope (SEM) images, including AT and TC files (Figure S1). The cell number quantification showed that the mutation of *SIM* and *SMR2* did not affect the epidermal cell number. The *smr1* mutant displayed an additional TC number, whereas the cell number in the AT files was unchanged compared to WT, indicating that SMR1 limits cell division in TC files (Figure 3A and B). Moreover, the AT and TC cell numbers were significantly increased in the *sim smr1* double mutant, suggesting that SIM and SMR1 function redundantly in controlling the hypocotyl epidermal cell division. Furthermore, the hypocotyl epidermal cell number was slightly recovered in the *sim smr1 smr2* triple mutant, suggesting that *SMR2* might work antagonistically with *SIM* and *SMR1* in controlling hypocotyl epidermal cell division.

We also investigated the effects of *ccs52a1* and *ccs52a2* loss-of-function mutants on the hypocotyl epidermal cell numbers. The data showed that a mutation in *CCS52A1* did not affect the epidermal cell number, while the TC number in the *ccs52a2* mutant

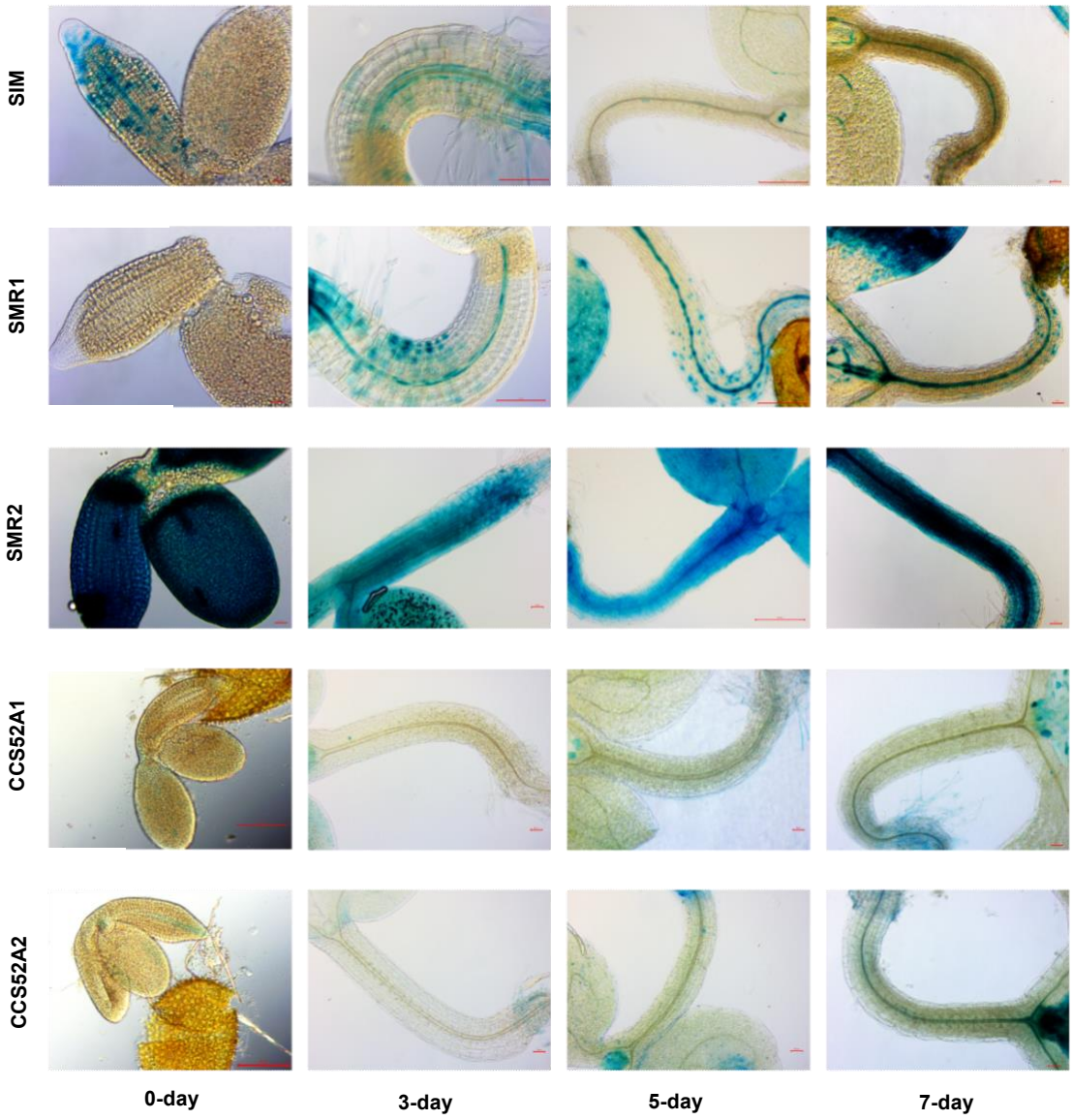

Figure 1 | Expression patterns of *SIM*, *SMR1*, *SMR2*, *CCS52A1*, and *CCS52A2* in light-grown hypocotyls. GUS activity of *SIM*, *SMR1*, *SMR2*, *CCS52A1*, and *CCS52A2* reporter lines in the *Arabidopsis* light-grown hypocotyls, visualized at the indicated time points. Scale bars=50 μm.

was increased compared to WT (Figure 3B). We also checked the hypocotyl epidermal cell number of the *sim ccs52a1* and *smr1 ccs52a1* double mutants. The data showed that these two mutants both generated additional cells of AT and TC files, indicating that CCS52A1 redundantly cooperates with SIM and SMR1 in controlling the cell number of AT and TC files (Figure 3).

2.2 | Difference in hypocotyl endoploidy under light- and dark-grown conditions

To investigate the effects of the endocycle-related genes on hypocotyl endoreplication, we compared the differences in endoploidy level of WT and mutant hypocotyls via flow cytometry (Figure 4 and Figure S2). Results showed that the *sim*, *smr1,* and *smr2* single mutants exhibited slight changes in endoploidy levels compared to WT under both light- and dark-grown conditions. The *sim smr1* double mutant displayed a significant decrease in endoploidy levels compared to both WT and the parent lines, and the *sim smr1 smr2* triple mutant displayed an exacerbated endoploidy defect. This suggests that *SIM*, *SMR1*, and *SMR2* play overlapping roles in regulating hypocotyl endoreplication.

The mutation in *CCS52A1* resulted in a reduction of endoploidy levels in both light- and dark-grown hypocotyls compared to WT. Light-grown hypocotyls of the *sim ccs52a1* double mutant showed no changes in endoploidy levels compared to WT. However, an endoploidy defect was observed in etiolated hypocotyls of the *sim ccs52a1* double mutant. These results indicate that *SIM* and *CCS52A1* interact to control hypocotyl endoreplication under dark-grown conditions. The flow cytometric results from the *smr1 ccs52a1* double mutant showed a reduction in endoreplication compared to WT under both light- and dark-grown conditions, with a further decrease in endoploidy levels observed in the dark-grown hypocotyls of *smr1 ccs52a1* compared to *ccs52a1*. These findings indicate that SMR1 cooperates with CCS52A1 in regulating hypocotyl cell endoreplication and that darkness enhances this effect.

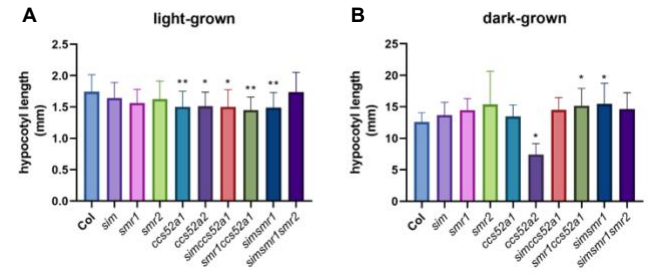

Figure 2 | Hypocotyl length of endocycle-related gene mutants. Analysis of hypocotyl length of WT and the endocycle-related gene mutants *sim*, *smr1*, *smr2*, *ccs52a1*, *ccs52a2*, sim *ccs52a1*, *smr1 ccs52a1*, *sim smr1*, and *sim smr1 smr2* under light- (A) and dark (B)-grown conditions at the 7-day time point. Data represent mean +SD (n>18, "none parametric" one-way ANOVA, p<0.05, one asterisk; p<0.01, two asterisks).

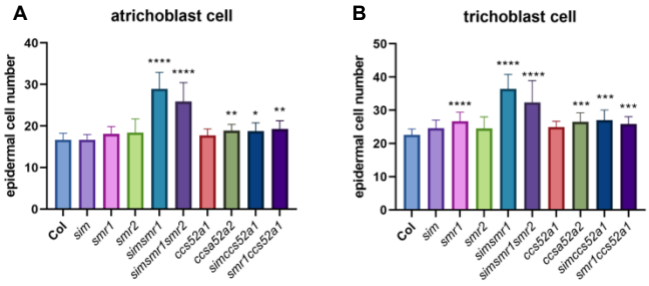

Figure 3 | Effects of these endoreplication-related genes on hypocotyl epidermal cell number. Quantification of 7-day-old hypocotyl epidermal cells of endocycle-related gene mutants compared to WT under light-grown conditions, including AT (A) and TC files (B). Data represent mean +SD (n=12 to 17 of each genotype, "none-parametric" one-way ANOVA, p<0.05, one asterisk; p<0.01, two asterisks; p<0.001, three asterisks; p<0.0001, four asterisks).

Flow cytometric results showed that the mutation of *CCS52A2* promoted endoreplication under dark-grown conditions, but not under light-grown conditions (Figure 4). This indicates that the light signal might be involved in the hypocotyl endoreplication caused by *CCS52A2*. In addition, the expression of *CCS52A1* and *CCS52A2* was not detected in the etiolated hypocotyls either (Figure 5A and B). Thus, how these two genes regulate the growth of hypocotyl under light- and dark-grown conditions remains elusive. As no viable *ccs52a1 ccs52a2* double mutant could be obtained [39], we used the *ccs52a1 DEL1*^{OE} line to mimic a *ccs52a1 ccs52a2* double mutant [24]. Because *DEL1* was identified as the specific repressor of CCS52A2, the *ccs52a1 DEL1*^{OE} line lacks *CCS52A1* function and has reduced the expression of *CCS52A2* [24]. The hypocotyl length of *ccs52a1 DEL1*^{OE} was close to the *ccs52a2* mutant, still shorter than WT (Figure 5C). Additionally, the endoploidy analysis of *ccs52a1 DEL1*^{OE} dark-grown hypocotyls was closer to *ccs52a1*, lacking the 16C-peak (Figure 5D). This suggests that *CCS52A1* is the major activator of APC/C complex in the hypocotyl, whereas *CCS52A2* mainly regulates hypocotyl elongation.

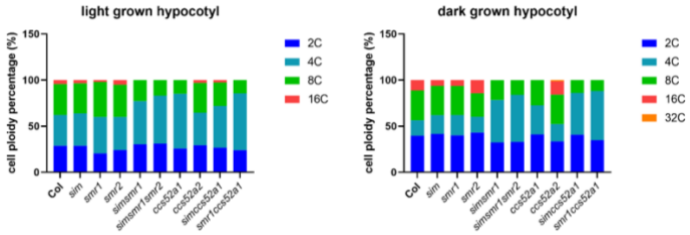

Figure 4 | Endoploidy analysis of WT and endocycle-related gene mutants' hypocotyl. Endoploidy analysis of WT and mutants hypocotyls under light (left)- and dark (right)-grown conditions at the 7-day time point. Data are representative of three biological repeats.

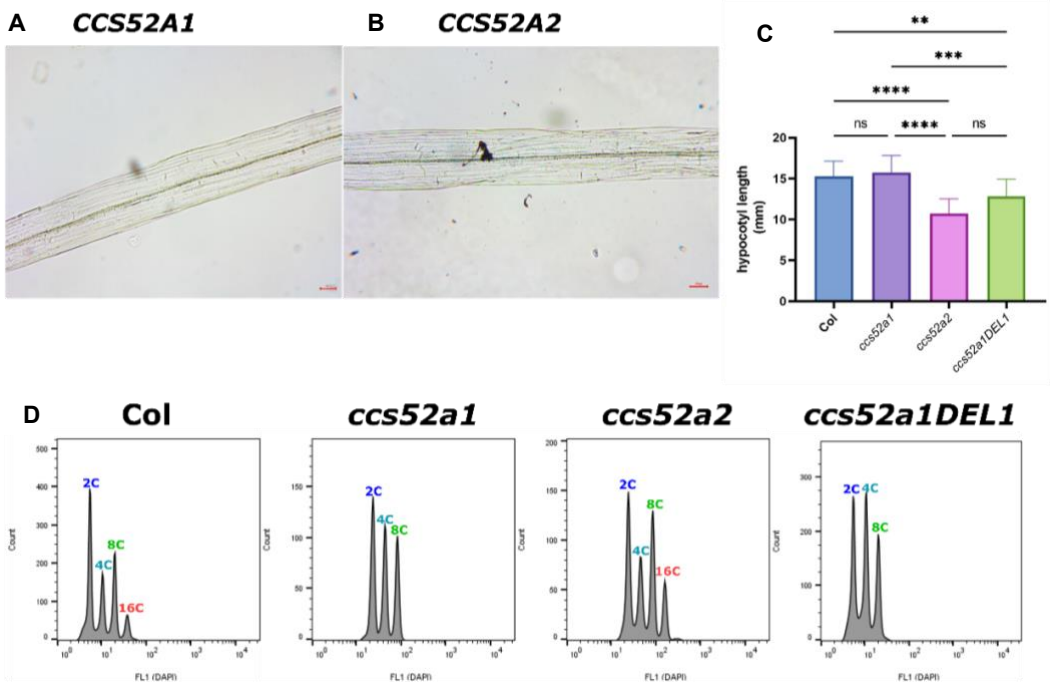

Figure 5 | Analysis on dark-grown *ccs52a1*, *ccs52a2*, *ccs52a1 DEL1OE*, and WT hypocotyls. GUS activity of *CCS52A1* (A) and *CCS52A2* (B) in 7-day-old etiolated hypocotyls. Analysis of the etiolated hypocotyl length of WT, *ccs52a1*, *ccs52a2*, and *ccs52a1 DEL1OE* at the 7-day time point (C). Data represent mean +SD (n>20, "parametric" one-way ANOVA, p<0.0001, four asterisks). Flow cytometric results from the dark-grown hypocotyls of WT, *ccs52a1*, *ccs52a2*, and *ccs52a1 DEL1OE* at the 7-day time point (D). The x-axis represents the DNA content, which was stained by DAPI, and the y-axis represents the counted cells. Scale bars=50 μm.

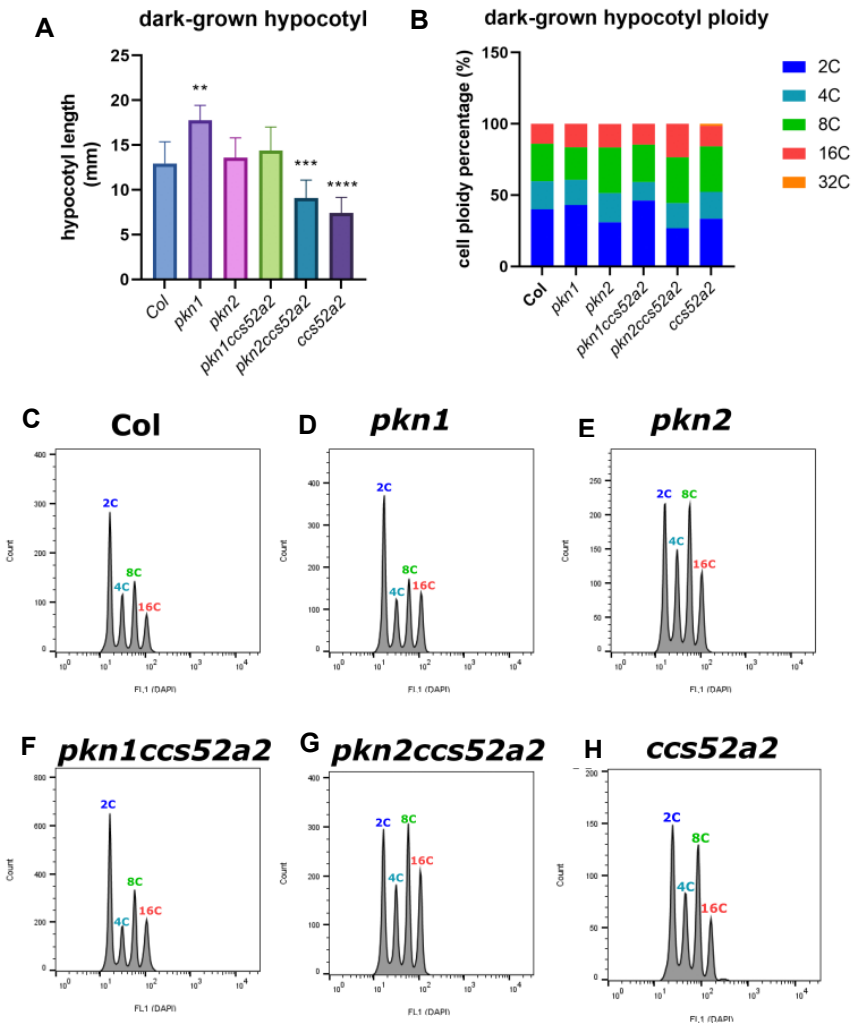

Figure 6 | Effects of PKN1 and PKN2 on hypocotyl elongation and endoreplication. Hypocotyl length analysis of WT, *pkn1*, *pkn2*, *pkn1 ccs52a2*, *pkn2 ccs52a2*, and *ccs52a2* under dark-grown conditions (A). Data represent mean +SD (n>11 from three independent biological repeats, "none parametric" one-way ANOVA, p<0.01, two asterisks; p<0.001, three asterisks; p<0.0001, four asterisks). Endoploidy analysis of dark-grown hypocotyl at 7-day time point (B), which is examined in ratio percentage. Flow cytometric results from the 7-day-old etiolated hypocotyls of WT (C), *pkn1* (D), *pkn2* (E), *pkn1 ccs52a2* (F), *pkn2 ccs52a2* (G), and *ccs52a2* (H). The x-axis represents the DNA content, which was stained by DAPI, and the y-axis represents the counted cells.

Previously, we identified that *PKN1* (AT2G43990) and *PKN2* (CYCA3;4) are the downstream targets of APC/C^{CCS52A2} complex [22,23]. To investigate the effects of PKN1 and PKN2 on hypocotyl elongation, we checked the hypocotyl length of the *pkn1*, *pkn2*, *pkn1 ccs52a2*, *pkn2 ccs52a2*, and ccs52a2 mutants under dark-grown conditions. The data showed that the mutation in *PKN1* promoted hypocotyl elongation, while no changes in hypocotyl length were detected in *pkn2*. In addition, *pkn1* was found to rescue the short hypocotyl in *ccs52a2*, while the hypocotyl length of the *pkn2 ccs52a2* double mutant was still shorter than that of WT (Figure 6A). These results indicate that PKN1 might be involved in the CCS52A2 pathway in regulating hypocotyl elongation.

Interestingly, analysis of endoploidy showed that the ploidy level of *pkn1* dark-grown hypocotyls was unchanged compared to WT, while *pkn2* displayed an increase in the hypocotyl endoploidy level. This indicates that *PKN1* is not involved in regulating the hypocotyl endoreplication process. Interestingly, the mutation in *PKN1* recovered the enhanced endoploidy level in the *ccs52a2* mutant hypocotyl, while the hypocotyl of the *pkn2 ccs52a2* mutant still exhibited a higher endoploidy level compared to WT (Figure 6B). These indicate that *PKN1* and *PKN2* inhibit hypocotyl elongation and endoreplication, respectively.

2.3 | Morphological study on the hypocotyl epidermal and cortex cells of endocycle-related mutants

To investigate the effects of the endocycle-related gene mutants on hypocotyl growth at the cellular scale, we used MGX to measure cell volume changes in the hypocotyl epidermal and cortex cell layers of these mutants under light-grown conditions (Figure 7). The results showed that most of these mutants displayed a reduction in cell volume in the hypocotyl AT, TC, and cortex cells (CC), while the *ccs52a2* knock-out line displayed no difference in cell volume compared to WT. Additionally, the AT files of *sim* displayed a slight increase in cell volume compared to that of WT. The *sim smr1* double mutant showed a more pronounced reduction than either of their parent lines in cell volume in the hypocotyl epidermal and cortex cells, while the cell volume reduction was a bit recovered in the *sim smr1 smr2* triple mutant. This suggests that *SIM* and *SMR1* play redundant roles in

regulating hypocotyl cell expansion, while *SMR2* may work antagonistically with *SIM* and *SMR1* in this process. The mutation in *CCS52A1* did not affect AT volume but reduced expansion in the TC and CC files, indicating that *CCS52A1* is not involved in the AT expansion mechanism.

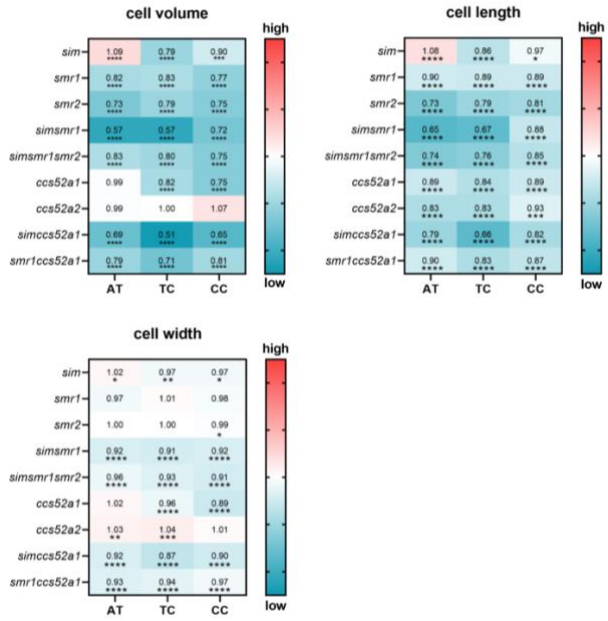

Figure 7 | Geometry analysis of light-grown hypocotyls. The analysis is conducted on atrichoblast cells (AT), trichoblast cells (TC), and cortex cells (CC) of 7-day-old hypocotyls of WT and endocycle-related gene mutants, including cell volume, length, and width. Value represents the ratio of each mutant to WT, which is visualized as heat map. The red color represents higher ratio value, whereas the blue color represents a lower ratio value (n>400 cells from three biological repeats, "non-parametric" one-way ANOVA, p<0.05, one asterisk; p<0.01, two asterisks; p<0.001, three asterisks; p<0.0001, four asterisks).

The *sim ccs52a1* double mutant showed a significant decrease in AT volume and an enhanced reduction in cell volume in the TC and CC cells compared to WT. These data suggest that SIM and *CCS52A1* may function redundantly in regulating hypocotyl cell expansion. In addition, the cell volume of *smr1* was smaller than WT in the AT, TC, and CC cells, while a similar reduction in cell volume was observed in the *smr1 ccs52a1* mutant. This suggests that *SMR1* is the main factor in regulating hypocotyl cell expansion. To determine which geometric factor, length or width, caused the cell volume changes, we performed the 3D CellAtlas function in MGX on these mutants and WT hypocotyls (Figure 7). The data showed that these changes occurred in cell length, not width, indicating that the mutations in these genes (*SIM*, *SMR1*, *SMR2*, *CCS52A1*, and *CCS52A2*) affect hypocotyl cell longitudinal expansion. The cell length of *ccs52a2* was significantly decreased, but it was slightly wider than WT. This can explain why the cell volume of the *ccs52a2* mutant was unchanged.

The effects of darkness on the hypocotyl elongation of endocycle-related gene mutants were examined (Figure 8). It has been suggested that darkness promotes hypocotyl elongation through the induction of additional rounds of endoreplication [2]. In order to evaluate the cellular parameters of these mutants (except *sim smr1 smr2*), an MGX analysis was performed. The etiolated hypocotyl was divided into three sections: top, middle, and bottom. The data showed that the TC volume of the *sim* mutant was significantly reduced in the top part, while the changes in the middle and bottom parts were insignificant. In addition, the cell volume in the AT and CC files was not significantly influenced. The cells at the top part of the *smr1* mutant hypocotyl appeared smaller than WT, whereas the hypocotyl cell volume of *smr1* appeared unchanged compared to WT. However, the TC and CC file volumes of *smr1* in the bottom part became much larger. The *sim smr1* double mutant showed enhanced hypocotyl cell expansion in the top and middle parts, while the AT volume in the bottom part showed a significant decrease, confirming again that SIM and SMR1 may play redundant roles in controlling hypocotyl cell expansion. The TC volume of the *smr2* mutant showed a decrease in the top part, while the bottom part of the hypocotyl cells also appeared larger compared to WT. This indicates that, in darkness, SMR2 may inhibit hypocotyl cell expansion in the bottom part.

The mutation of *CCS52A1* had no impact on the top and middle parts of the etiolated hypocotyl cells. However, in the bottom part, the *ccs52a1* mutant led to larger TC and CC volume files compared to WT, while there were no significant changes observed in the volume of AT files. Additionally, the volume of the hypocotyl cells in the *ccs52a2* mutant remained unchanged compared to WT. The double mutants of *sim ccs52a1* and *smr1 ccs52a1* both exhibited smaller cells in the top (AT, TC, and CC) and middle (TC and CC) parts of the dark-grown hypocotyl; however, the cell volume of the middle AT files remained unchanged compared to WT. In the *sim ccs52a1* mutant, no significant changes in cell volume were observed in the bottom part of the hypocotyl cells. In the *smr1 ccs52a1* mutant, the bottom TC files were larger than WT, while the volume of AT and CC files remained unchanged.

In conditions of darkness, similar to light-grown conditions, the cell length was found to be the primary factor that influenced the cell volume. The average cell length in the top part of the hypocotyl showed a reduction compared to WT in the mutants under investigation. This reduction was consistent with the changes in cell volume observed in the top and middle parts. The cell length of the *sim smr1* and *sim ccs52a1* double mutant, as well as *smr1 ccs52a1,* exhibited greater defects compared to WT, except for the AT middle part of the *sim ccs52a1* and *smr1 ccs52a1* double mutants. Additionally, the dark-grown *ccs52a2* hypocotyl cells were shorter than WT, particularly in the top and bottom parts, while at the same time they were wider than WT. This result further reinforces the hypothesis that *CCS52A2* influences the longitudinal and transverse expansion of the hypocotyl cells.

2.4 | Difference in cell wall composition in *ccs52a1* and *ccs52a2* hypocotyls

Lignin, a major component of the secondary cell wall, generally restricts cell expansion [40]. An investigation was performed to determine if lignin biosynthesis may be responsible for the observed reduction in longitudinal expansion of *ccs52a2* hypocotyl cells. We performed Basic Fuchsin (BF) and Wiesner staining protocols [41,42] on light-grown hypocotyls of WT, *ccs52a1* (a homolog of *CCS52A2* in the *Arabidopsis* genome), and *ccs52a2*. The results of the BF and Wiesner staining revealed increased lignin content in the *ccs52a2* light-grown hypocotyl compared to both WT and *ccs52a1* (Figure 9A). However, these staining methods were not effective in the dark-grown hypocotyls, making it difficult to determine whether the *ccs52a2* dark-grown hypocotyl cells have increased lignin content.

The lignin biosynthesis in *Arabidopsis* is controlled by several enzymes, such as phenylalanine ammonia-lyase (PAL), cinnamate 4-hydroxylase (C4H), 4-coumarate: CoA ligase (4CL), cinnamoyl-CoA reductase (CCR), cinnamyl alcohol

dehydrogenase (CAD), and caffeic acid O-methyltransferase (COMT) [43]. In this study, we analyzed the expression levels of these genes in the light- and dark-grown hypocotyls of WT, *ccs52a1*, and *ccs52a2* at the 7-day time point (Figure 9B and C). The transcriptional results revealed that the expression level of *PAL1* was upregulated in the *ccs52a2* hypocotyl compared to that of WT and *ccs52a1* under both light- and dark-grown conditions. Furthermore, under dark-grown conditions, the difference in expression level of *PAL1* in *ccs52a2* was enhanced compared to WT and *ccs52a1* (Figure 9C), which might be attributed to the enhanced hypocotyl elongation defect in the etiolated *ccs52a2* mutant.

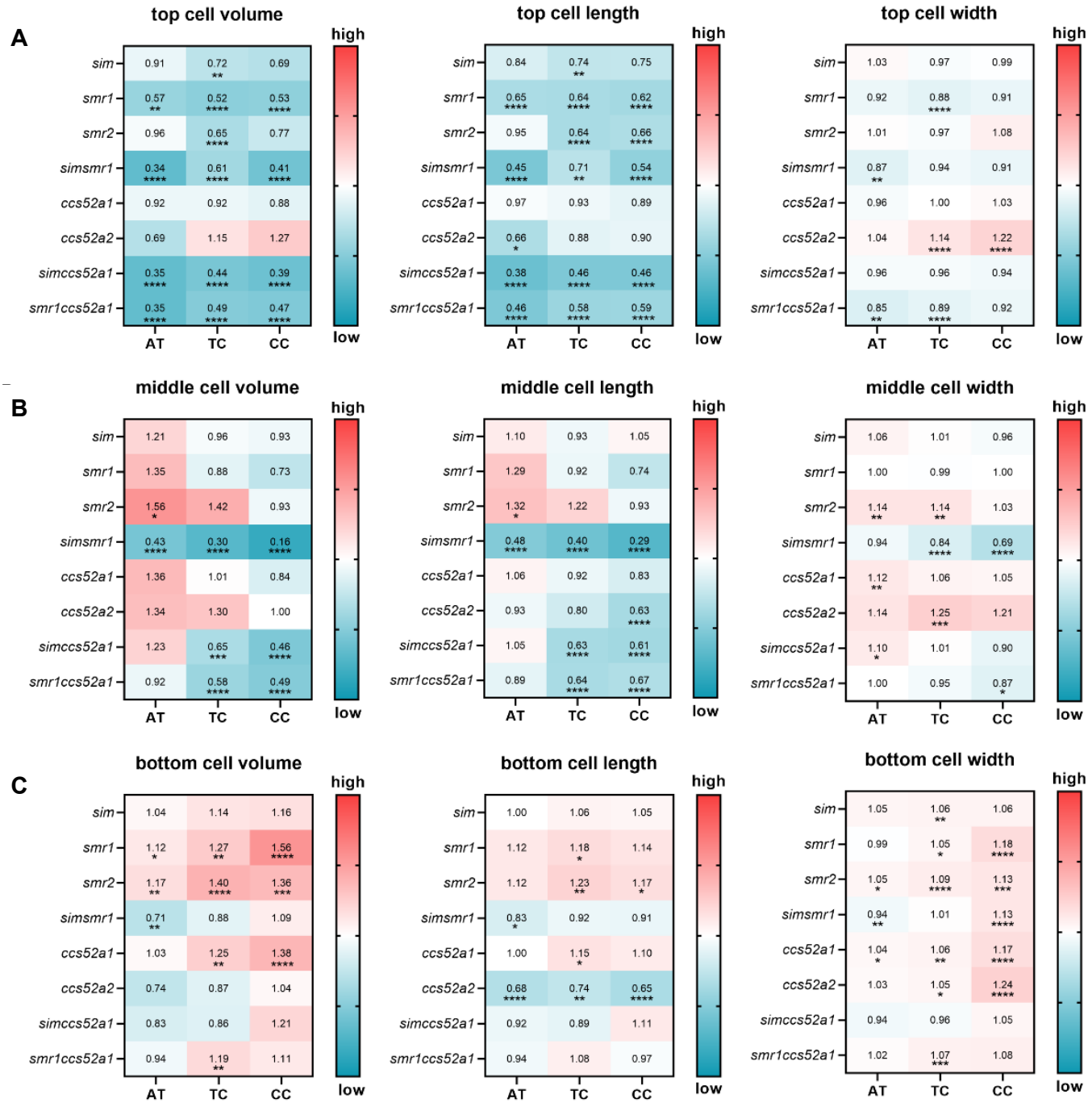

Figure 8 | Geometrical analysis of dark-grown hypocotyls. Differences in cell volume, length, and width upon 3D cell stack analysis for atrichoblast cell (AT), trichoblast cell (TC), and cortex cell (CC) of WT and endocycle-related mutants under dark-grown conditions. The data are calculated from the top (a), middle (b), and bottom (c) parts of the hypocotyl. Value represents the ratio of each mutant to WT, which is visualized as a heat map. The red color represents a higher ratio value, whereas the blue color represents a lower ratio value (n=40 to 130 cells from two biological repeats, "non-parametric" one-way ANOVA, p<0.05, one asterisk; p<0.01, two asterisks; p<0.001, three asterisks; p<0.0001, four asterisks).

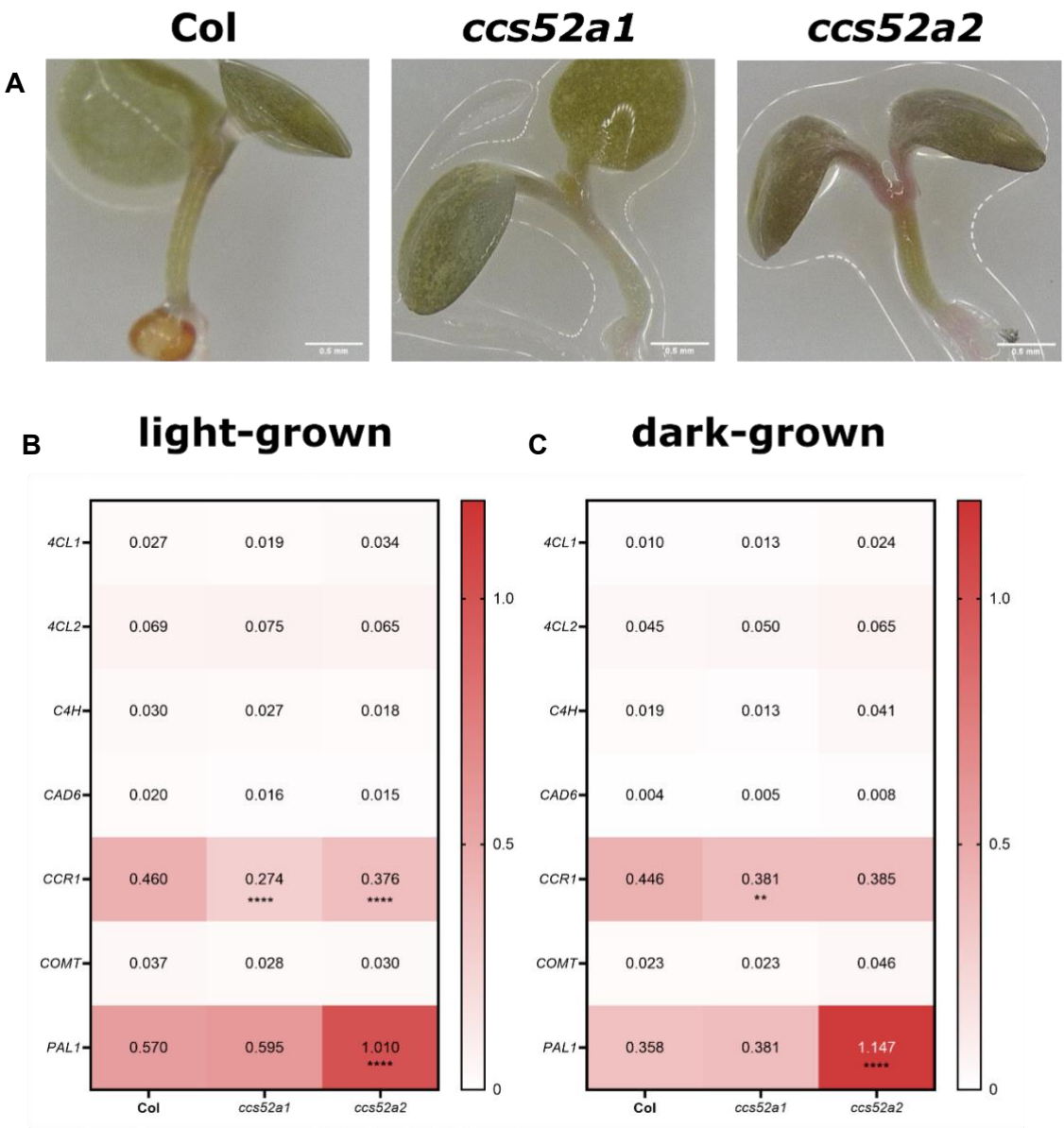

Figure 9 | Analysis of lignin in *ccs52a1*, *ccs52a2*, and WT light-grown hypocotyl. Analysis of lignin content in the WT, *ccs52a1*, and *ccs52a2* light-grown hypocotyls (from left to right) at the 7-day time point, which were stained by Wiesner (A). Relative expression level of lignin biosynthesis genes in the hypocotyls of WT, *ccs52a1*, and *ccs52a2* that grew under light- (B) and dark-grown (C) conditions. The red color represents an increase in expression level compared to WT plants. Data represent the mean of the expression level of each gene (p<0.01, two asterisks; p<0.0001, four asterisks).

3 | DISCUSSION

Arabidopsis hypocotyl epidermal cells are commonly used as a research model for endoreplication studies, as they are easily characterized and endoreplication occurs in the epidermal cells, particularly under dark-grown conditions, without cell division [2]. *SIM/SMR1* and *CCS52A1/2* have been identified as the primary positive regulators of the *Arabidopsis* endoreplication [14–16]. *SMR2*, another member of the SMR family, has been found to play a similar role to *SIM* and *SMR1* in regulating the transition from mitosis to endocycle in the *Arabidopsis* leaves [18]. However, the effects of these genes on hypocotyl development have not been thoroughly studied. In this study, we analyzed the endoploidy level and cell volume of endocycle-related gene mutants (*sim*, *smr1*, *smr2*, *ccs52a1*, *ccs52a2*, *sim ccs52a1*, *smr1 ccs52a1*, *sim smr1*, and *sim smr1 smr2*) and ectopic expressed *SIM* and *CCS52A2* in the hypocotyl epidermal cells with the *pCER6* promoter, an epidermis-specific gene, under light- and dark-grown conditions. Meanwhile, we utilized several methods to investigate the changes in cell wall activities, trying to link the potential relationship between endoreplication and cell wall mechanics.

3.1 | *SIM*, *SMR1*, and *SMR2* have overlapping roles in controlling the growth of the hypocotyl

The single mutations of *SIM*, *SMR1*, and *SMR2* showed minimal alterations in the length of the hypocotyl under both light- and dark-grown conditions. However, the *sim smr1* double mutant exhibited a distinct deviation in hypocotyl length, with shorter and longer lengths observed under light- and dark-grown conditions, respectively (Figure 2). This suggests a redundant role for *SIM* and *SMR1* in the regulation of hypocotyl elongation and the

involvement of light signals in this process. In addition, the hypocotyl length of the *sim smr1 smr2* triple mutant remained unchanged compared to WT under both light- and dark-grown conditions.

The single mutations of *SIM*, *SMR1*, and *SMR2* had a limited impact on the number of hypocotyl epidermal cells compared to WT. However, the changes were more pronounced in the *sim smr1* and *sim smr1 smr2* mutants. Results obtained through flow cytometry indicated that the mutations in *SIM*, *SMR1*, and *SMR2* did not affect the endoploidy level of the hypocotyl under both light- and dark-grown conditions (Figure 4). On the other hand, a gradual increase in endoreplication defects was observed in the hypocotyl of the *sim smr1* and *sim smr1 smr2* mutants under both light- and dark-grown conditions. This suggests that SIM, SMR1, and SMR2 perform overlapping functions in regulating hypocotyl cell growth, including cell number and endoreplication. Similar results have been reported in the *Arabidopsis* leaves, where an increased endoploidy defect was observed in the *sim smr1 smr2* triple mutant compared to WT and the single mutants [18].

Cell volume analysis under light-grown conditions showed a reduction in the cell volume of the hypocotyl in the *sim*, *smr1*, and *smr2* single mutants compared to the control, suggesting positive roles of *SIM*, *SMR1*, and *SMR2* in controlling hypocotyl cell expansion. Meanwhile, an increase in the cell volume of *sim* AT files was observed compared to WT, indicating a negative role for SIM in regulating cell expansion in the hypocotyl AT files under light-grown conditions. The epidermal cell volume (AT and TC files) of the *sim smr1* double mutant was approximately 57% of WT, while the ratio of the epidermal cell volume in the *sim smr1 smr2* triple mutant to WT was around 80%. In addition, the number of hypocotyl epidermal cells in the *sim smr1 smr2* triple mutant showed some recovery compared to the *sim smr1* double mutant. These data suggest that SMR2 might act antagonistically to SIM and SMR1 in controlling the cell number and expansion of the hypocotyl epidermal cells. Cell expansion is considered to be a result of endoreplication [2]. However, the relationship between endoreplication and cell volume in these single mutants (*sim*, *smr1*, and *smr2*) is uncoupled, indicating that SIM, SMR1, and SMR2 may regulate cell expansion without affecting the endoploidy level in the *Arabidopsis* hypocotyl. The changes in endoreplication and cell volume were found to be consistent in the *sim smr1* and *sim smr1 smr2* mutants' hypocotyl.

3.2 | *CCS52A2* promotes hypocotyl elongation

Analysis of the *ccs52a1* mutant revealed a marginal impact on hypocotyl length but a substantial reduction in endoploidy levels under both light- and dark-grown conditions when compared to WT. In contrast, the *ccs52a2* mutant displayed shorter hypocotyls, particularly under dark-grown conditions, and slight changes in endoploidy levels compared to WT, and even an increase in endoreplication was observed under dark-grown conditions. The etiolated hypocotyl of *ccs52a1 DEL1*^{OE}, to mimic the *ccs52a1 ccs52a2* double mutant, displayed decreased endoploidy level, like *ccs52a1*, and reduced hypocotyl length, like *ccs52a2*. These findings indicate that *CCS52A1* is the major factor of hypocotyl endoreplication, while *CCS52A2* mainly functions in hypocotyl elongation under dark-grown conditions. However, the phenotypic changes in *ccs52a1*/*a2* mutants contrast with their weak expression level in hypocotyls, with a primary presence in the vascular cells.

The mutations in *CCS52A1* and *CCS52A2* have been found to affect the tissue organization in the root, resulting in longer root meristem zone and a disorganized quiescent center (QC), respectively [15]. In addition, the root growth of *ccs52a2* was repressed, including reduced root length, meristem size, cortical cell number, and cell size [23]. Given that seedlings rely on the absorption of nutrients to support hypocotyl growth during the post-germination stage, the observed changes in endoreplication and elongation of the etiolated hypocotyl of *ccs52a1* or *ccs52a2* might be attributed to their root growth defect.

CELLULOSE SYNTHASE-LIKE D5 (*CSLD5*), which is localized in the cell plated during the M phase, has been identified as a downstream target of *CCS52A2* [44]. However, the role of CCS52A2 in regulating cell wall activities remains unclear. The staining done by Basic Fuchsin and Wiesner revealed an increase in lignin content of the light-grown *ccs52a2* mutant hypocotyls compared to WT and *ccs52a1*. Lignin, which works as the major component of the secondary cell wall, can enhance plant cell wall thickness and represses cell expansion [40,45]. In *Arabidopsis*, polyploidy was found to repress lignin biosynthesis compared to the diploid line [36]. These findings indicate that lignin biosynthesis has a potential link with cell cycle mechanisms. The transcripts of *PAL1*, a gene crucial for lignin biosynthesis in *Arabidopsis* [40], were upregulated in the hypocotyls of the *ccs52a2* mutant under both light-grown and dark-grown conditions. In the *Arabidopsis* genome, *PAL1* and *PAL2* encode phenylalanine ammonia-lyase (PAL; EC 4.3.1.5), which plays an initial step in the Phenylpropanoid and Flavonoid Pathways [46]. The expression pattern of *PAL1* has been reported to display a decrease in expression levels in the hypocotyls of light-grown plants during the post-germination stage [47]. In addition, the PAL activity in the hypocotyl is repressed under dark-grown conditions [48]. These data suggest that *CCS52A2* might participate in the hypocotyl elongation via repressing the expression of *PAL1*, particularly under dark-grown conditions.

Figure 10 | A model for *CCS52A2* functions in hypocotyl elongation. During post-germination stage, *CCS52A2* positively contributes to hypocotyl elongation via inhibiting the expression of lignin biosynthesis genes. Defective hypocotyl elongation can be rescued by the *pkn1* mutant, indicating that *PKN1* acts as the downstream target of *CCS52A2* in controlling hypocotyl elongation. The relationship between *PKN1* and lignin biosynthesis remains elusive.

Potential evidence was found in the hypocotyl of the *reduced epidermal fluorescence 5* (*ref5-2*) mutant, an allele of *CYP83B1*, which encodes the oxime-metabolizing enzyme [49]. The data showed that the hypocotyl length of *ref5-2* is longer than WT with a decrease in PAL activity, indicating that PAL may negatively regulate hypocotyl elongation [50]. The *Arabidopsis* encodes two isoforms:PAL1 and PAL2 [51]. However, a substantial reduction in lignin content was only observed in the *pal1 pal2* double mutant [51], which supports plant cell expansion.

PKN1 and *PKN2* have been identified as downstream targets of the *APC*/*C*^{CCS52A2} complex [22,23], which mutations can partially restore endoreplication and cell division defects in the root of *ccs52a2*. We investigated the roles of *PKN1* and *PKN2* in hypocotyl elongation and endoreplication. The data showed that, under dark-grown conditions, the *pkn1* mutant has a longer hypocotyl than WT and can restore the hypocotyl defect in the *ccs52a2* mutant. Whereas the hypocotyl of the *pkn2 ccs52a2*

double mutant was still shorter compared to WT. These results suggest that, in the *Arabidopsis* hypocotyl, PKN1 might be involved in the CCS52A2 pathway regulating hypocotyl elongation. Additionally, PKN1 was identified to localize at microtubule structures during the M phase [22]. However, since hypocotyl cells mainly remain at the endoreplication stage, the function of PKN1 in the hypocotyl cell plate/wall remains unclear (Figure 10).

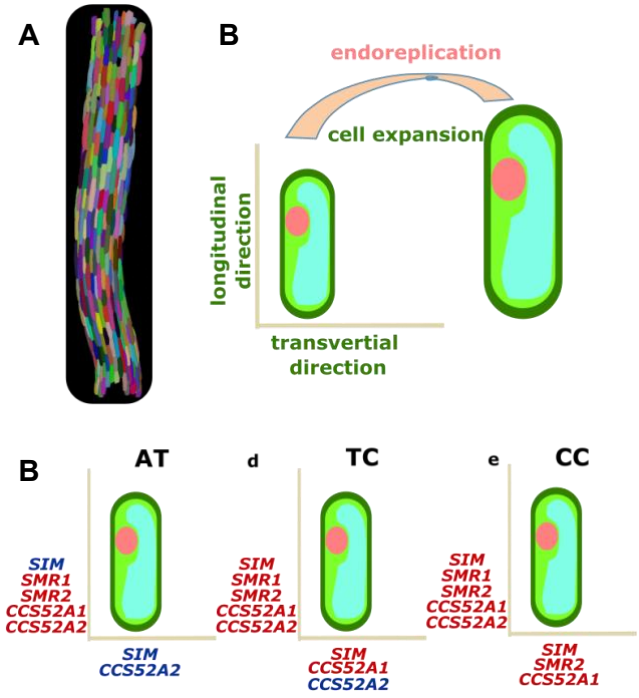

Figure 11 | Visual representation for *SIM/SMRs* and *CCS52A1/2* contribution to hypocotyl cell expansion under light-grown conditions. A light-grown hypocotyl, which is annotated by MGX, at the 7-day time point (A). During hypocotyl growth, the hypocotyl epidermal cells undergo endocycle and undergo cell expansion in longitudinal and transversal directions (B). *SIM/SMRs* and *CCSS52A1/A2* play positive (red) or negative (blue) roles in regulating AT (c), TC (D), and CC (E) files of hypocotyl expansion in longitudinal and transversal directions.

3.3 | SIM/SMRs and CCS52A1/2 regulate hypocotyl cell expansion in different directions

The MGX data, under light-grown conditions, showed that SIM/SMRs and CCS52A1/2 modulate hypocotyl cell expansion in a tissue-specific manner (Figure 11). In general, these genes positively contribute to longitudinal expansion of hypocotyl cells, as a reduction in cell length was observed in these gene single mutant hypocotyls. However, in AT files, SIM negatively controls AT file expansion in both the longitudinal and transversal directions (Figure 11C). CCS52A2 represses transversal expansion in AT and TC files, which may explain why no difference in cell volume was observed in the *ccs52a2* mutant hypocotyl. In addition, SIM and CCS52A1 were found to positively regulate transversal expansion in TC and CC files (Figure 11D and E). In CC files, *SMR2* also promotes transversal expansion of cells (Figure 11E).

Similarly, the hypocotyls of the *sim smr1* double mutant and the *sim smr1 smr2* triple mutants showed enhanced defects in longitudinal expansion compared to either parent mutant line. In addition, *sim smr1* showed shorter cell length than the *sim smr1 smr2* triple mutant. These results confirm again that SIM and SMR1 function redundantly in hypocotyl development, while SMR2 functions antagonistically with SIM and SMR1.

Darkness promotes hypocotyl elongation, which accentuates differences in geometric parameters. Meanwhile, analyzing whole hypocotyl cellular data under dark-grown conditions can be difficult. To address this, we divided the dark-grown hypocotyl into three parts: top, middle, and bottom. Our data showed that the reduction in cell volume mainly occurred in the top part of the dark-grown hypocotyl. In the bottom part, some exceptions were found; for example, the TC volume in the bottom part hypocotyl of *smr1* and *smr2* was bigger than WT. Geometrical analysis revealed that the cell length of the bottom TC files significantly increased in *smr1* and *smr2* compared to WT under dark-grown conditions, whereas in light, the TC of *smr1* and *smr2* appeared shorter than WT. This indicates that these genes might regulate cell expansion in a light-dependent manner.

3.4 | *CCS52A2* promotes cell expansion via light pathway

Flow cytometric results from the *pCER6:CCS52A2* hypocotyl, which specifically expressed *CCS52A2* in hypocotyl epidermal cells, showed that CCS52A2 promotes endoreplication in hypocotyl epidermal cells under both light- and dark-grown conditions. In addition, the light-grown pCER6:CCS52A2 hypocotyl epidermal cells were enlarged, while no such changes were observed under dark-grown conditions. This data indicates that the cell endoreplication and expansion are uncoupled in the dark-grown *pCER6:CCS52A2* hypocotyl. This result indicates that cell endoreplication and expansion triggered by CCS52A2 might be in two parallel pathways, with the effect of CCS52A2 on cell expansion relying on light signals. Another explanation could be that under dark-grown conditions, CCS52A2 triggers cell expansion later than endoreplication. A similar phenotype was observed in *Arabidopsis* in later stage collet hair cells, where endoreplication precedes cell expansion [52]. Therefore, we still need to analyze the dark-grown *pCER6:CCS52A2* hypocotyl at additional time points, such as 5 and 9 days, in order to fully understand the process.

4 | CONCLUSION

In this study, we mainly analyzed the relationships between endoreplication and cell expansion in the *Arabidopsis* hypocotyl. The flow cytometric results, without a tissue-specific marker, can only represent the endoploidy levels of whole hypocotyl cells. Therefore, we may cross the *pCER6* marker line, which is especially expressed in the hypocotyl epidermal cells, with coordinated mutants to specially sort the hypocotyl epidermal cells. Alternatively, we may apply tissue-specific knockout technology to specifically analyze the endoploidy level changes caused by SIM/SMRs and *CCS52A1/A2*. We still need additional work to figure out the potential relationship between lignin and *CCS52A2* in hypocotyl growth. Thus, we will cross lignin biosynthesis gene mutants with the *ccs52a2* mutant to see if the hypocotyl elongation defective phenotypes can be recovered. *PKN1* appeared to be responsible for *ccs52a2* short hypocotyl under dark-grown conditions; whether PKN1 is involved in the lignin biosynthesis pathway needs to be figured out. Meanwhile, we will conduct immunolocalization analyses on cross-sections of hypocotyls from *pCER6:SIM* and *pCER6:CCS52A2* to identify the specific cell layers where cell wall modifications occur. We also need additional analysis at different time points of dark-grown *pCER6:CCS52A2* lines, to figure out whether *CCS52A2* could promote hypocotyl cell expansion under dark-grown conditions.

5 | MATERIALS AND METHODS

5.1 | Plant material, growth conditions, and chemical treatments

In this study, we used *Arabidopsis thaliana* lines in the Columbia-0 (Col-0) background. The specific lines used were *sim*, *smr1*, *smr2*, *sim smr1*, *sim smr1 smr2*, *ccs52a1* (Salk_083656), *ccs52a2*, *sim ccs52a1*, *smr1 ccs52a1*, *pkn1*, *pkn2*, *pkn1 ccs52a2*, *pkn2 ccs52a2*, *ccs52a1 DEL1*^{OE}, *pCER6*, *pCER6:SIM*, and *pCER6:CCS52A2*. The plants were grown on a sugar-free medium consisting of 1/2 Murashige and Skoog (MS) medium supplemented with 1% plant agar and 0.5 g/L MES at pH 5.8. The seeds were sterilized and plated on the medium, then stratified in the dark for three days at 4°C. After stratification, the seeds were transferred to a growth room with a 16-hour light/8-hour dark cycle (70 µmol $m^{-2}s^{-1}$) at 22°C for seven days. For dark treatment, the plates were wrapped in aluminum foil and kept in the same growth room [53].

5.2 | Confocal microscopy

Samples were cleared and fixed using the ClearSee protocol [54], and cell walls were counterstained with Calcofluor White to enable visualization of cellular boundaries. Confocal imaging was performed using a Zeiss LSM 710 laser-scanning microscope equipped with a 40× water-immersion objective lens (NA 0.8), allowing high-resolution acquisition of optical sections.

5.3 | 3D analysis by MGX

3D image segmentation and analysis were performed using MorphoGraphX (version 2.0) [55,56]. Raw image stacks were first smoothed using a Gaussian blur (x = 0.6, y = 0.6, z = 0.3), followed by cell segmentation with an ITK threshold value of 1000. Segmentation errors were manually corrected to ensure accuracy. A 3D cellular mesh was generated with a cube size of 1.0, and geometric parameters, including cell volume, length, and width, were quantified using the “heatmap” analysis tool in MorphoGraphX.

5.4 | GUS Staining

Transcriptional and translational reporter lines were first incubated in 80% ice-cold acetone for 30 min, followed by gentle washing. A phosphate buffer was prepared by mixing 14 mL of 100 mM NaH_2PO_4, 36 mL of Na_2HPO_4, and 50 mL of distilled water. Seedlings were washed in this phosphate buffer for 5–10 min, and the wash step was repeated three times. The X-Gluc staining solution was prepared by combining 98 mL of phosphate buffer with 2 mM potassium ferricyanide, 2 mM potassium ferrocyanide, and 1 mL of X-Gluc. Seedlings were incubated in this solution at 37°C in the dark (wrapped in aluminum foil) overnight. After staining, seedlings were cleared in ethanol at room temperature overnight, followed by clearing in lactic acid for 30–60 minutes. Stained samples were mounted in a few drops of lactic acid and imaged under a microscope.

5.5 | Flow cytometry analysis

Flow cytometry analysis was performed on mutant and transgenic lines, in which nuclei were stained with DAPI. The proportion of GFP-positive nuclei was quantified to determine the endopolyploidy level in hypocotyl epidermal cells from 7-day-old seedlings grown under both light and dark conditions

5.6 | Lignin staining on seedlings

Lignin deposition in *Arabidopsis* seedlings was assessed using Wiesner staining and Basic Fuchsin (BF) staining. For Wiesner staining, 7-day-old seedlings were incubated in Wiesner reagent (1% phloroglucinol dissolved in 100 mL of 95% ethanol and 16 mL of 37% HCl), and lignification was evaluated visually as previously described [42]. For BF staining, seedlings were processed using the ClearSee protocol and subsequently incubated in 0.2% Basic Fuchsin in ClearSee for at least 1 h, followed by one rinse in fresh ClearSee and a second incubation for 30 min or longer before imaging [41].

5.7 | Materials preparation for Comprehensive Microarray Polymer Profiling (CoMPP)

The hypocotyls of 7-day-old light-grown *pCER6* transgenic lines were excised and flash-frozen in liquid nitrogen. The frozen tissue was homogenized in a 2 mL Eppendorf tube using a metal bead. The homogenized material was extracted sequentially with 70% ethanol, a 1:1 mixture of methanol and chloroform, and acetone. For each extraction step, the samples were thoroughly vortexed, centrifuged at maximum speed for 10 min, and the supernatant discarded. After the final acetone wash, the Eppendorf tubes were left open to air-dry on the bench overnight. The dried extracts were weighed, ensuring a minimum of 5 mg per sample.

5.8 | Extraction of cell wall glycans

The dried extracts were resuspended by adding 500 µL of 50 µM CDTA (pH 7.5) to each sample. The tubes were briefly vortexed and homogenized using a TissueLyser for 30 s at 20 Hz, followed by 2h at 8 Hz. Samples were centrifuged for 1 min at maximum speed, and the supernatant was carefully collected into a new Eppendorf tube and stored at 4 °C. The remaining pellets were washed with 500 µL of 4 M NaOH containing 0.1% (w/v) $NaBH_4$, homogenized again using the TissueLyser for 30 s at 20 Hz and 2h at 8 Hz, centrifuged for 1 min at maximum speed, and the supernatant was collected and stored at 4 °C. The pellets were subsequently washed with 500 µL of cadoxen solution (31% v/v 1,2-diaminoethane with 0.78 M CE), and the supernatant was collected following the same procedure. For downstream analyses, the extracted solutions were diluted to 1:2 and 1:20 concentrations.

9.9 | Printing Microarrays

For immunoassay analysis, 5 µL of each sample (diluted 1:2 and 1:20) was loaded onto appropriately prepared cut arrays, with three technical replicates per sample. Each sample was labeled manually with a pencil. Arrays were blocked with 5% skimmed milk powder in TBST [Tris-buffered saline (20 mM Tris-HCl, 140 mM NaCl, pH 7.5) with 0.1% Tween-20] for 1 h with gentle shaking. Primary cell wall antibodies, diluted 1:100 in blocking solution, were applied to the arrays and incubated for 1.5 h under gentle agitation. Arrays were then washed three times with TBST for 5 min each under gentle shaking. Subsequently, secondary antibodies, diluted 1:1000 in blocking solution, were applied and incubated for 1.5 h with gentle shaking, followed by a repeat of the washing procedure.

5.10 | BCIP/NBT colorimetric quantification of array signals

The BCIP/NBT color development solution was prepared by adding 200 µL of substrate to 10 mL of buffer (0.1 M Tris-HCl, 0.1

M NaCl, 0.05 M $MgCl_2$). This solution was applied to the washed arrays, which were incubated with gentle shaking in the dark until visible color development occurred. Afterward, the arrays were allowed to air-dry on the bench. The signal intensity was quantified by measuring the integrated grey density of each spot.

ACKNOWLEDGEMENTS

We are grateful to our colleagues for their support and discussion. This work was supported by a scholarship to L.L. from the China Scholarship Council (CSC) and a Bijzonder Onderzoeksfonds (BOF) grant from Ghent University.

AUTHOR CONTRIBUTIONS

Conceptualization: L.L. and T.K | Methodology: L.L. | Investigation: L.L. | Writing – original draft: L.L. | Writing – review and editing: T.K. The authors confirm their contributions to the paper.

DATA AVAILABILITY STATEMENT

All the data generated or analyzed during this study are included in this published article and its supplementary information files at https://trendsacademics.com/tpb/index.php/ojs/article/view/2/2.

CONFLICTS OF INTEREST

The authors declare no conflicts of interest.

REFERENCES

1. Vandenbussche F, Vriezen WH, Smalle J, Laarhoven LJJ, Harren FJM, Van Der Straeten D. **2005**. Of light and length: Regulation of hypocotyl growth in *Arabidopsis*. *BioEssays* 27:275–284
2. Gendreau E, Traas J, Desnos T, Grandjean O, Caboche M, Höfte H. **1997**. Cellular basis of hypocotyl growth in *Arabidopsis thaliana*. *Plant Physiology* 114:295–305
3. Kudo N, Kimura M, Matsuoka M. **2004**. Endoreduplication cycles during hypocotyl growth of cabbage (*Brassica oleracea* L.) under light and dark conditions. *Plant Biotechnology* 21:295–312
4. Daher FB, Chen Y, Bozorg B, Clough J, Jönsson H, Braybrook SA. **2018**. Anisotropic growth is achieved through the additive mechanical effect of material anisotropy and elastic asymmetry. *eLife* 7:1–28
5. Narukawa H, Yokoyama R, Komaki S, Sugimoto K, Nishitani K. **2015**. Stimulation of cell elongation by tetraploidy in hypocotyls of dark-grown *Arabidopsis* seedlings. *PLoS ONE* 10:1–13
6. Collett CE, Harberd NP, Leyser O. **2000**. Hormonal interactions in the control of *Arabidopsis* hypocotyl elongation. *Plant Physiology* 124:553–561
7. Derbyshire P, Findlay K, McCann MC, Roberts K. **2007**. Cell elongation in *Arabidopsis* hypocotyls involves dynamic changes in cell wall thickness. *Journal of Experimental Botany* 58:2079–2089
8. De Lucas M, Davière JM, Rodríguez-Falcón M, Pontin M, Iglesias-Pedraz JM, Lorrain S, Fankhauser C, Blázquez MA, Titarenko E, Prat S. **2008**. A molecular framework for light and gibberellin control of cell elongation. *Nature* 451:480–484
9. Lin W, Zhou X, Tang W, Takahashi K, Pan X, Dai J, Ren H, Xia X, Xu G. **2021**. TMK-based cell-surface auxin signalling activates cell-wall acidification. *Nature* 599:278–282
10. Ren H, Santner A, del Pozo JC, Murray JAH, Estelle M. **2018**. A subset of plasma membrane-localized PP2C.D phosphatases negatively regulate SAUR-mediated cell expansion in *Arabidopsis*. *PLoS Genetics* 14:1–27
11. Du M, Spartz AK, Gray WM. **2022**. Biphasic control of cell expansion by auxin coordinates etiolated seedling development. *Science Advances* 8:1–13
12. Ishida T, Adachi S, Yoshimura M, Shimizu K, Sugiyama M, Hasebe M. **2010**. Auxin modulates the transition from the mitotic cycle to the endocycle in *Arabidopsis*. *Development* 137:63–71
13. Wu G, Cameron JN, Ljung K, Spalding EP. **2016**. *ABCB19*-mediated polar auxin transport modulates Arabidopsis hypocotyl elongation and the endoreplication variant of the cell cycle. *Plant Journal* 85:209–218
14. Walker JD, Oppenheimer DG, Concienne J, Larkin JC. **2000**. SIAMESE, a gene controlling the endoreduplication cell cycle in *Arabidopsis thaliana* trichomes. *Development* 127:3931–3940
15. Vanstraelen M, Baloban M, Da Ines O, Cultrone A, Lammens T, Boudolf V, Brown SC, De Veylder L, Mergaert P, Kondorosi E. **2009**. APC/CCCS52A complexes control meristem maintenance in the *Arabidopsis* root. *Proceedings of the National Academy of Sciences of the United States of America* 106:11806–11811
16. Churchman ML, Brown ML, Kato N, Kirik V, Hülskamp M, Inzé D, De Veylder L, Walker JD, Zheng Z, Oppenheimer DG, Genschik P, Larkin JC. **2006**. SIAMESE, a plant-specific cell cycle regulator, controls endoreplication onset in *Arabidopsis thaliana*. *Plant Cell* 18:3145–3157
17. Wang K, Chen Y, Chen Y, Liu Z, Li Y, Chen Y, Ding L, Zhang X, Liu Y, Liu J. **2020**. The CDK inhibitor SIAMESE targets both CDKA;1 and CDKB1 complexes to establish endoreplication in trichomes. *Plant Physiology* 184:165–175
18. Kumar N, Harashima H, Kalve S, Bramsiepe J, Wang K, Sizani BL, Jadamba L, Guan Y, Dissmeyer N, Gutierrez RA, Sugimoto K. **2015**. Functional conservation in the SIAMESE-RELATED family of cyclin-dependent kinase inhibitors in land plants. *Plant Cell* 27:3065–3080
19. Fülöp K, Tarayre S, Kelemen Z, Horváth G, Kevei Z, Nikovics K, Bakó L, Brown S, Kondorosi É, Szabados L. **2005**. *Arabidopsis* anaphase-promoting complexes: Multiple activators and wide range of substrates might keep APC perpetually busy. *Cell Cycle* 4:4084–4092
20. Lammens T, Boudolf V, Kheibarshekan L, Panagiotou S, Van Leene J, De Milde L, Van De Slijke E, De Rycke R, Inzé D, De Veylder L. **2008**. Atypical E2F activity restrains APC/CCCS52A2 function obligatory for endocycle onset. *Proceedings of the National Academy of Sciences of the United States of America* 105:14721–14726
21. Boudolf V, Lammens T, Boruc J, Van Leene J, Van Den Daele H, Maes S, Van Isterdael G, Russinova E, Kondorosi E, Witters E, De

Jaeger G, Inzé D, De Veylder L. **2009**. CDKB1;1 forms a functional complex with CYCA2;3 to suppress endocycle onset. *Plant Physiology* 150:1482–1493

22. Willems A, Heyman J, Huysmans M, De Veylder L. **2021**. The APC/CCCS52A2 E3-ligase complex targeted PKN1 protein is a plant lineage specific driver of cell division. *Plant Physiology* 191:1574-1595

23. Willems A, Friml J, Van de Velde K, Van de Cotte B, Van de Walle L, Van Leene J, De Jaeger G, De Veylder L. **2020**. The cyclin CYCA3;4 is a postprophase target of the APC/CCCS52A2 E3-ligase controlling formative cell divisions in *Arabidopsis*. *Plant Cell* 32:2979–2996

24. Heyman J, Cools T, Vandenbussche F, Veylder LD. **2017**. Tissue-specific control of the endocycle by the anaphase promoting complex/cyclosome inhibitors UVI4 and DEL1. *Plant Physiology* 175:303–313

25. Vlieghe K, Boudolf V, Beemster GTS, Maes S, Ormenese S, Van Isterdael G, Inzé D, De Veylder L. **2005**. The DP-E2F-like gene DEL1 controls the endocycle in *Arabidopsis thaliana*. *Current Biology* 15:59–66

26. Berckmans B, Lammens T, Van Den Daele H, Magyar Z, Bögre L, De Veylder L. **2011**. Light-dependent regulation of DEL1 is determined by the antagonistic action of E2Fb and E2Fc. *Plant Physiology* 157:1440–1451

27. Bhosale R, Boudolf V, De Veylder L. **2019**. Endoreplication as a potential driver of cell wall modifications. *Current Opinion in Plant Biology* 51:58–65

28. Jegu T, Latrasse D, Debernardi JM, Pumplin N, Veluchamy A, Wang L, Sureshkumar S, Velanis CN, Raynaud C, Gruissem W, Thirugnanasambantham K, Delannoy E, Benhamed M, Bergounioux C, Bowler C, Balzergue S, Domínguez-Ferreras A, Schneeberger K, Fletcher JC, Ecker JR, Gutierrez-Marcos J, Jacobsen SE, Palatnik JF, Coupland G, Turck F. **2013**. Multiple functions of Kip-related protein5 connect endoreduplication and cell elongation. *Plant Physiology* 161:1694–1705

29. Dukowic-Schulze S, Harris A, Li J, Sundararajan A, Mudge J, Retzel EF, Chen C. **2021**. UV-B irradiation results in inhibition of hypocotyl elongation, cell cycle arrest, and decreased endoreduplication mediated by miR5642. *Photochemistry and Photobiology* **(DOI: 10.1111/php.13574)**

30. Bhosale R, Maere S, Boudolf V, De Veylder L. **2018**. A spatiotemporal DNA endoploidy map of the *Arabidopsis* root reveals roles for the endocycle in root development and stress adaptation. *Plant Cell* 30:2330–2351

31. Urbanowicz BR, Peña MJ, Moniz HA, Moremen KW, York WS. **2014**. Two *Arabidopsis* proteins synthesize acetylated xylan in vitro. *Plant Journal* 80:197–206

32. Bensussan M, Lefebvre V, Verbancic J, Yang Y, Chen X, Kronenberger J, Beauclair L, Grandjean O, Marchive C, Brunoud G, Guyon V, Boucherez J, Thévenin J, Navarro L, Bouchez D, Höfte H. **2015**. Suppression of dwarf and irregular xylem phenotypes generates low-acetylated biomass lines in *Arabidopsis*. *Plant Physiology* 168:452–463

33. Perazza D, Herzog M, Hülskamp M, Brown S, Dorne AM, Bonhomme S. **1999**. Trichome cell growth in *Arabidopsis thaliana* can be derepressed by mutations in at least five genes. Genetics 152:461–476

34. Wang S, Gu Y, Zebell SG, Anderson LK, Wang W, Mohan R, Dong X. **2014**. A noncanonical role for the CKI-RB-E2F cell-cycle signaling pathway in plant effector-triggered immunity. *Cell Host and Microbe* 16:787–794

35. Hamdoun S, Zhang C, Gill M, Kumar N, Churchman M, Larkin JC, Kwon A, Lu H, Lee JY. **2016**. Differential roles of two homologous cyclin-dependent kinase inhibitor genes in regulating cell cycle and innate immunity in *Arabidopsis*. *Plant Physiology* 170:515–527

36. Corneillie S, De Storme N, Vanhee C, Vandamme N, De Bruyne M, De Rycke R, Geelen D, Boerjan W, Vanholme B. **2019**. Polyploidy affects plant growth and alters cell wall composition. *Plant Physiology* 179:74–87

37. Ma Y, Chuat JC, Li J, Voiniciuc C, Li H, Zhao X, Wang Y, Zhang Y, Wu J, Liu L, Wang X, Liu X, Zhang X, Wang H, Li J, Zhang J, Wang Y, Liu X. **2022**. Endoreplication mediates cell size control via mechano-chemical signaling from cell wall. *Science Advances* 8:eabq2047

38. Boron AK, Vissenberg K. **2014**. The *Arabidopsis thaliana* hypocotyl, a model to identify and study control mechanisms of cellular expansion. *Plant Cell Reports* 33:697–706

39. Baloban M, Vanstraelen M, Tarayre S, Reuzeau C, Cultrone A, Mergaert P, Kondorosi E. **2013**. Complementary and dose-dependent action of AtCCS52A isoforms in endoreduplication and plant size control. *New Phytologist* 198:1049–1059

40. Liu Q, Luo L, Zheng L. **2018**. Lignins: Biosynthesis and biological functions in plants. *International Journal of Molecular Sciences* 19:335

41. Sexauer M, Geldner N, Vermeer JEM. **2021**. Visualizing polymeric components that define distinct root barriers across plant lineages. *Development* 148:dev195123

42. Van de Wouwer D, Decou R, Audenaert D, Beeckman T, De Rycke R, Hoebeke L, Boerjan W, Vanholme B. **2016**. Chemical genetics uncovers novel inhibitors of lignification, including p-iodobenzoic acid targeting CINNAMATE-4-HYDROXYLASE. *Plant Physiology* 172:198–220

43. Xie M, Zhang J, Li H, Wu J, Liu L, Wang X, Zhang X, Wang H, Li J, Zhang J. **2018**. Regulation of lignin biosynthesis and its role in growth-defense tradeoffs. *Frontiers in Plant Science* 9:1427

44. Gu F, Nielsen E. **2016**. *Arabidopsis* CSLD5 functions in cell plate formation in a cell cycle-dependent manner. *Plant Cell* 28:1722–1737

45. Vaahtera L, Schulz J, Hamann T. **2019**. Cell wall integrity maintenance during plant development and interaction with the environment. *Nature Plants* 5:924–932

46. Kubasek WL, Shirley BW, McKillop A, Goodman HM, Briggs W, Ausubel FM. **1992**. Regulation of flavonoid biosynthetic genes in germinating *Arabidopsis* seedlings. *Plant Cell* 4:1229–1236

47. Ohl S, Hedrick SA, Chory J, Lamb CJ. **1990**. Functional properties of a phenylalanine ammonia-lyase promoter from *Arabidopsis*. *Plant Cell* 2:837–848

48. Kubo H. **2007**. Promoter activity of phenylalanine ammonia-lyase gene of Pharbitis nil in *Arabidopsis*. *Journal of Plant Biochemistry and Biotechnology* 16:109–111

49. Hansen CH, Wittstock U, Olsen CE, Hick AJ, Pickett JA, Halkier BA. **2001**. CYP83B1 is the oxime-metabolizing enzyme in the

glucosinolate pathway in *Arabidopsis*. *Journal of Biological Chemistry* 276:24790–24796

50. Kim JI, Dolan WL, Anderson NA, Chapple C. **2015**. Indole glucosinolate biosynthesis limits phenylpropanoid accumulation in *Arabidopsis* thaliana. *Plant Cell* 27:1529–1546
51. Rohde A, Morreel K, Ralph J, Goeminne G, Hostyn V, De Rycke R, Cushman J, Boerjan W. **2004**. Molecular phenotyping of the pal1 and pal2 mutants of *Arabidopsis thaliana* reveals far-reaching consequences on phenylpropanoid, amino acid, and carbohydrate metabolism. *Plant Cell* 16:2749–2771
52. Sliwinska E, Mathur J, Bewley JD. **2015**. On the relationship between endoreduplication and collet hair initiation and tip growth, as determined using six *Arabidopsis thaliana* root-hair mutants. *Journal of Experimental Botany* 66:3285–3295
53. Decaestecker W, Buono RA, Pfeiffer ML, Vangheluwe N, Jourquin J, Karimi M, Van Isterdael G, Beeckman T, Nowack MK, Jacobs TB. **2019**. CRISPR-TSKO: A technique for efficient mutagenesis in specific cell types, tissues, or organs in *Arabidopsis*. *Plant Cell* **(DOI: 10.1105/tpc.19.00454)**
54. Kurihara D, Mizuta Y, Noguchi T, Higashiyama T. **2015**. ClearSee: A rapid optical clearing reagent for whole-plant fluorescence imaging. *Development* 142:4168–4179
55. Montenegro-Johnson TD, Stamm P, Strauss S, Topham AT, Tsagris M, Wood ATA, Smith RS, Bassel GW. 2015. Digital single-cell analysis of plant organ development using 3DCellAtlas. *Plant Cell* 27:1018–1033
56. Wolny A, Cerrone L, Vijayan A, Tofanelli R, Barro AV, Louveaux M, Wenzl C, Strauss S, Kreshuk A, Hamprecht FA. **2020**. Accurate and versatile 3D segmentation of plant tissues at cellular resolution. *eLife* 9:e57613